Observations on Thermospheric and Mesospheric Density Disturbances Caused by Typhoons and Convective Storms

R. J. Hung,* Y. D. Tsao,† and C. C. Lee‡
University of Alabama in Huntsville, Huntsville, Alabama 35899
D. L. Johnson§
NASA Marshall Space Flight Center, Huntsville, Alabama
and
A. J. Chen,¶ C. H. Lin,** and J. J. Pan††
National Central University, Chung Li, Taiwan, Republic of China

The vhf radar and hf Doppler sounder located at the subtropical and low-latitude observing site of Taiwan has been used to observe atmospheric parameters from the troposphere, to the middle atmosphere, and then to the thermosphere, during the time passage of typhoons and tropical storms. For observations at mesospheric heights, time-dependent wind velocities with three-dimensional profiles are deduced from the Doppler spectra of vhf radar returns, whereas gravity waves are detected in the backscattered power, radial velocities, and Doppler spectral width. For observations at thermospheric heights, time-dependent phase-path change of hf radio waves reflected from ionospheric heights is used to measure Doppler frequency variation of gravity-wave parameters. Propagation characteristics of the gravity waves excited by the enhanced convective motions of typhoons and tropical storms were detected from the Fourier power spectrum analysis of the three-dimensional wind velocities from the radial velocities of multiple beams of the vhf radar and the phase-path variations of Doppler sounding of hf radio waves reflected from the ionosphere, together with their cross-correlation analysis. The density perturbations caused by the propagation of the gravity waves due to typhoons and tropical storms were calculated from both the vhf radar and hf Doppler sounder observations. These short-term middle atmospheric and thermospheric density changes are key elements needed for space vehicle design purposes. Projects such as the Space Shuttle, Shuttle II, Shuttle C, Tethered Satellite, Hubble Space Telescope, Aerobraking Orbital Transfer Vehicle, and Aeroassisted Flight Experiment will benefit from such studies.

I. Introduction

RECENTLY, the National Central University (NCU) of Taiwan has installed a vhf radar and an hf Doppler sounder at its subtropical and low-latitude observing site. The vhf phase-coherent radar measures the amplitude and Doppler shift of radio waves that are scattered back to the receiving antennas. The application of vhf radar in the observations of the troposphere, stratosphere, and mesosphere has been reviewed by Balsley and Gage,[1] Gage and Balsley,[2] Rottger,[3] and others. The hf Doppler sounder has been widely used in the study of traveling ionospheric disturbances (TID), which are manifestations of gravity waves propagating through the ionosphere.[4-6] During the time periods of convective motion, TID have been observed in the thermosphere. In a study by Williams et al.,[7] simultaneous observations of a TID by means of incoherent scatter radar and other radio techniques were reported. Their results indicate that the TID wave parameters deduced from these observations are in good agreement with the acoustic-gravity wave-dispersion relation.

By using vhf radar networks, one can observe the following atmospheric parameters: 1) three-dimensional wind by using multiple beams or by beam swinging[8]; 2) turbulence intensity by measuring the backscattered power[9-11] or by deriving the width of the autocorrelation function for the wind[12,13]; 3) frequency, horizontal wavelength, vertical wavelength, and phase velocity of gravity waves by measuring the frequency of the horizontal and vertical wind velocity variations from multiple beams of the vhf radars and their cross-correlation analysis[14-16]; 4) tropopause height from deriving the information on sharp changes in the atmospheric static stability by looking for specular reflection[17]; 5) frontal zone structure and convergence of the wind field before cloud formation by measuring the amplitude and Doppler shift of the backscattered power of the vhf radar[18,19]; and 6) the vertical temperature profile by using vhf radar with special sensitivity to temperature structure.[20,21]

TID observed in the thermosphere have been closely related to the convective storms in the troposphere. In particular, gravity waves associated with tornado activity[22,23] and hurricanes/typhoons[24,25] have been observed with an hf CW Doppler array system. By using a ray-tracing technique, Hung et al.[26,27] have shown that the enhanced convection-initiated gravity waves associated with tornadoes were generated by thunderheads embedded in a squall line and/or from isolated clouds with intense convection,[28-30] whereas gravity waves associated with hurricanes/typhoons were excited by the convection motion of all clouds of the storms.[24,25] Large-scale TIDs, which are excited near the aurora zone during the time period of high geomagnetic activity characterized by a high K_p index, can be observed at the thermospheric heights.[5,22]

Received Nov. 7 1988; presented as Papers 89-0765 and 89-0854 at the AIAA 27th Aerospace Sciences Meeting, Reno, NV, Jan. 9-12, 1989; revision received June 15, 1989.

*Professor. Associate Fellow AIAA.
†Research Engineer.
‡Graduate Student; currently, Research Engineer.
§Staff Scientist.
¶Professor.
**Associate Professor.
††Graduate Student.

Clearly, the upward flux of waves at the stratosphere and mesosphere is a function of the production of gravity waves in the troposphere.[31,32] The probable tropospheric gravity-wave sources are perhaps unstable wind shear, topography, and convection. Wind shear produces waves with phase velocities characteristic of tropospheric wind speeds, whereas topography generates gravity waves with a phase-velocity distribution centered about zero. Of the three dominate gravity-wave sources, the phase-velocity spectrum associated with convection is the least understood. Severe convective storms provide a significant portion of momentum and energy to excite gravity waves associated with convection.

Gravity waves also play an important role in the coupling between the lower and upper atmospheres. Gravity waves observed in the ionosphere have been traced to sources mostly in the troposphere.[22,33,34] Sources of gravity waves can be determined by using ray-tracing computations.[23,26,27,30]

Gravity waves are responsible for the perturbation of atmospheric density. Short-term density variability is generated by the propagation of gravity waves, which are detected by the backscattered echo power and the Doppler spectral width of the signal returns of the vhf radar[35] at mesosphere, and the phase-path variations of Doppler sounding of hf radio waves reflected from ionosphere.[22]

In this study, the vhf radar Doppler array systems located at Chung Li, Taiwan, were used to observe three-dimensional wind speeds and gravity waves, and to determine the density perturbations at different heights of mesosphere and thermosphere during the time period of typhoons and tropical storm activities.

II. VHF Radar Observations of Mesospheric Density Disturbances During the Time Period of Typhoon Activity

A. Meteorological Background

The tropical storm was gradually formed in the South China Sea during the last week of May 1988. At 0540 Greenwich mean time (GMT), May 30, 1988, Typhoon Susan was formed at 200 km northwest of Luzon, the Philippines. It moved in a north-northwesterly direction and gradually increased in storm intensity. At 1500 GMT, May 31, Typhoon Susan turned to the northeast and moved toward Taiwan. Susan hit Henchun, Taiwan, at approximately 2340 GMT, June 1. At 0000 GMT, June 2, Susan swept over southern Taiwan and moved into the Pacific Ocean. It moved in a northeasterly direction and gradually decreased. At 0100 GMT, June 3, Susan disappeared east of Okinawa. Figure 1 shows the locations and the times of the Typhoon Susan storm track from May 30 to June 3, 1988. Figure 2 shows the infrared satellite imagery at 0018 GMT, June 2, 1988.

Surface meteorological data show that the area of low pressure was located at the Korean Peninsula and the Yellow Sea. There was a cold front that extended from the Yellow Sea in a southwesterly direction to the Pacific Ocean east of Taiwan. There were two areas of low pressure located at Tibet and southwest Mongolia. Central and southwest China were covered by high pressure. There was another high-pressure area located 1200 km east of Japan that moved easterly. Figure 3 shows a 850 mb weather map at 0000 GMT, June 2, 1988.

Satellite infrared imagery shown in Fig. 2 also shows that there was an intense disturbance of intertropical convergence zone (ITCZ) located in the equatorial area. The activity of Typhoon Susan made the connection of ITCZ and the cold

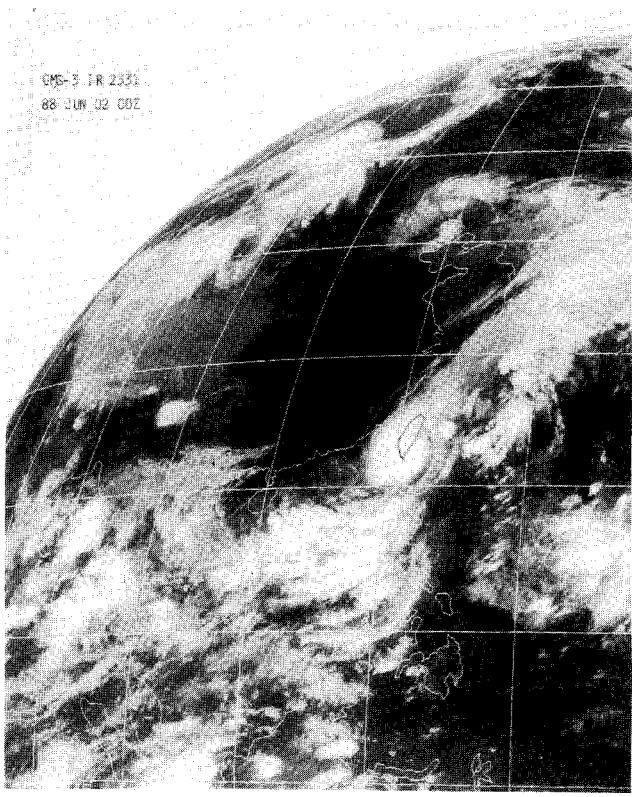

Fig. 2 Satellite imagery of Typhoon Susan with the storm track over Taiwan at 0000 GMT, June 2, 1988.

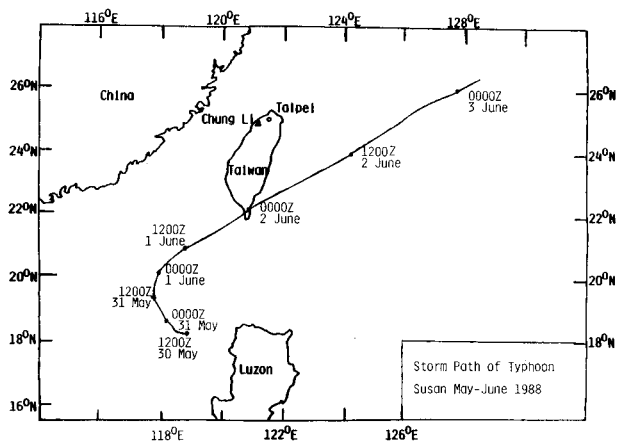

Fig. 1 Locations and times of the Typhoon Susan storm track on May 30-June 2, 1988.

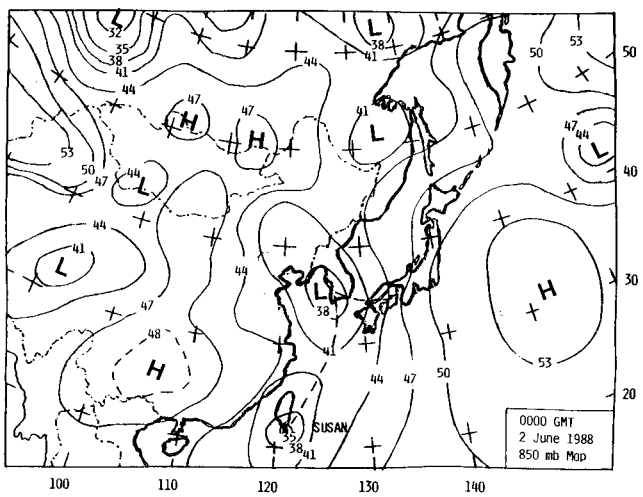

Fig. 3 850-mb weather map of the Far East area at 0000 GMT, June 2, 1988.

Table 1 Three-dimensional wind speeds observed via vhf radar during tropical storm activity[a]

	Height, km								
	76.4			79.5			92.2		
	Wind speed, m/s			Wind speed, m/s			Wind speed, m/s		
Time, GMT	v_x	v_y	v_z	v_x	v_y	v_z	v_x	v_y	v_z
7.47	−2.11	1.31	−1.07	−2.09	−0.68	−1.01	−5.61	−5.14	−0.27
7.48	−1.25	0.63	−1.06	−1.36	−0.23	−0.87	−3.97	−3.86	−0.43
7.48	−2.07	1.56	−0.69	−2.49	0.83	−0.51	−3.25	−2.48	−0.22
7.49	−2.80	3.81	−0.82	−3.08	3.14	−0.77	−2.33	−0.48	−0.24
7.50	−2.64	3.25	−0.56	−2.56	2.52	−0.65	−1.72	−0.99	−0.31
7.50	−1.58	2.78	−0.72	−1.81	0.55	−0.49	−2.58	−2.36	−0.11
7.51	−0.21	0.98	−0.47	−1.20	−1.22	−0.12	−3.33	−2.31	−0.16
7.52	−2.63	0.20	−0.37	−2.91	−1.11	0.21	−1.68	−0.78	0.21
7.52	−2.38	−0.58	0.36	−1.89	−1.81	0.70	−0.20	−0.44	1.01
7.53	−2.08	−2.63	0.20	−1.11	−3.08	0.36	2.12	−1.21	0.80
7.54	−3.04	−2.44	0.23	−1.99	−2.79	0.18	1.26	0.22	−0.06
7.55	−1.95	−1.28	−0.09	−1.18	−1.33	−0.05	0.99	1.49	−0.22
7.55	−2.88	−0.57	−0.08	−2.23	−1.22	−0.05	0.12	0.23	−0.22
7.56	−2.36	−1.68	−0.32	−2.08	−2.00	−0.59	−0.34	0.01	−0.71
7.57	−3.57	−3.45	−0.11	−2.92	−4.26	−0.17	−0.19	−2.00	−0.57
7.57	−3.82	−3.06	−0.24	−2.66	−4.29	−0.53	−1.16	−0.85	−0.68
7.58	−3.94	−3.24	−0.58	−3.50	−4.69	−0.80	−1.38	−0.68	−0.41
7.59	−2.77	−3.00	−0.62	−2.83	−4.83	−0.84	−2.22	−1.15	−0.31
7.59	−0.82	−3.05	−0.67	−1.52	−4.98	−0.73	−2.64	−1.59	0.16
8.00	−0.39	−3.38	−1.25	−1.50	−4.70	−1.40	−1.28	−2.77	−0.64
8.01	−2.36	−2.94	−1.42	−3.94	−4.29	−1.36	−3.72	−3.35	−0.53
8.01	−1.23	−4.27	−1.54	−3.27	−4.90	−1.49	−2.83	−4.06	−0.12
8.02	−1.50	−6.43	−1.03	−2.60	−6.61	−0.87	−1.01	−5.77	0.13
8.03	−0.93	−6.91	−1.11	−1.42	−6.75	−1.06	−1.20	−6.23	0.08
8.03	−0.32	−7.46	−0.86	−1.24	−7.59	−0.53	−0.48	−6.20	0.62
8.04	1.05	−8.17	−1.17	−0.41	−7.57	−0.95	−0.83	−4.73	0.59
8.05	0.19	−7.49	−0.74	−0.78	−6.32	−0.31	0.06	−4.31	0.94
8.05	0.53	−7.79	−0.26	−0.65	−5.14	0.02	0.41	−3.94	1.03
8.06	0.64	−7.21	−0.02	−0.25	−4.85	0.25	1.46	−4.56	1.06
8.07	−0.66	−5.86	0.11	−1.06	−3.18	0.26	2.05	−3.03	0.72
8.07	−3.28	−5.01	0.08	−3.79	−1.96	0.53	−0.70	−1.94	0.70
8.08	−2.25	−4.06	0.13	−1.46	−1.20	0.45	1.13	−1.27	0.59
8.09	−2.33	−3.20	0.33	−1.37	−1.57	0.69	0.70	−1.39	0.67
8.10	−1.69	−2.16	−0.27	−2.12	−1.53	0.04	−2.57	−0.93	0.23
8.10	−2.09	−1.08	−0.42	−2.76	−0.59	0.01	−2.44	0.54	0.05
8.11	−2.84	−0.97	−0.09	−2.90	0.34	0.02	−1.98	1.53	−0.41
8.12	−1.78	−0.55	0.20	−2.18	0.78	0.35	−1.75	1.65	−0.87
8.12	−1.12	−1.33	0.05	−2.21	0.35	0.04	−2.58	2.02	−1.35
8.13	0.62	−1.38	0.48	−0.30	−0.09	0.42	−1.97	2.47	−1.52
8.14	−0.06	−0.37	−0.13	−0.96	0.17	−0.24	−1.39	3.23	−2.06
8.14	0.14	0.14	0.04	−0.97	0.09	−0.17	−1.39	1.92	−2.09
8.15	3.00	0.04	0.15	1.93	−0.27	−0.32	0.71	3.13	−1.71

[a]Time: 0747–0815 GMT, May 27, 1988. Location: Chung Li, Taiwan.

frontal system that extended from the Yellow Sea. This interaction brought large quantities of moisture from the southeast and intensified the low pressure near the Korean Peninsula and Yellow Sea.

With these background conditions, one can anticipate observing gravity waves induced by strong convection in the troposphere and propagated to the mesosphere.[1,29]

B. Remote Sensing of Wind Velocity

From the backscattering echo power and the Doppler spectral width of the signal returns of the vhf radar, one can determine the wind velocities at different heights. To insure that meaningful observation data are obtained, the following basic parameters have been adopted in screening the good quality data to be used for the analysis: 1) strength of returned signal, 2) signal-to-noise ratio, and 3) comparison of spectral width with Gaussian distribution. The measurement of three-dimensional wind speeds can be accomplished by using either the spaced antenna method or the Doppler method, which are both available from the vhf radar located at Chung Li, Taiwan. Results of wind profiles deduced from vhf radar in the tropospheric heights have been compared with the rawinsonde observations at the same areas with good agreement.

From the signal returns of the vhf radar, one observes the Doppler spectrum of the backscattered power. From the analysis of the Doppler spectrum of the backscattered power, both radial-velocity Doppler spectral width and signal strengths are deduced. In this study, the Doppler method, which measures the Doppler shift of the scattered radar echoes at oblique incidence, was used in the analysis. The complex autocorrelation, or the spectral analysis, yields radial velocities v' at different directions. Assuming that the antenna beam points at a zenith angle δ and at an azimuth angle α, directed clockwise from the north, then

$$v' = v_x \sin\alpha \cdot \sin\delta + v_y \cos\alpha \cdot \sin\delta + v_z \cos\delta \qquad (1)$$

For a constant zenith angle, and assuming the wind field is uniform, v' will vary sinusoidally with the azimuth angle α. The Fourier analysis of the data series $v'(\alpha)$ directly yields the eastward wind v_x and the northward wind v_y from the Fourier coefficients, as well as the vertical velocity v_z. This is the so-called VAD method (velocity azimuth display).[36]

Three arrays with 64 yagi antennas each are installed at the National Central University (25°N, 121°E), Chung Li, Taiwan.[25] These antennas are arranged in such a way that three

Table 2 Three-dimensional wind speeds observed via vhf radar during typhoon Susan passage[a]

	Height, km								
	76.4			82.7			85.9		
	Wind speed, m/s			Wind speed, m/s			Wind speed, m/s		
Time, GMT	v_x	v_y	v_z	v_x	v_y	v_z	v_x	v_y	v_z
9.32	−9.57	4.13	−0.33	−10.37	3.72	−0.31	−6.98	5.27	0.02
9.33	−2.91	2.41	0.74	−4.48	2.74	1.27	−3.65	5.51	1.50
9.33	1.86	4.23	1.36	0.81	3.72	2.27	0.64	5.87	2.25
9.34	3.02	0.82	1.91	2.68	3.84	1.80	2.34	7.76	1.54
9.34	3.22	−1.44	1.81	3.99	0.36	1.52	3.14	4.06	0.54
9.35	3.07	−1.92	0.77	4.78	−2.58	0.86	3.48	−0.81	−0.39
9.36	−0.16	−3.62	−0.96	3.04	−5.96	−1.33	3.48	−4.03	−1.92
9.36	−5.47	−6.79	−1.73	−2.40	−9.22	−2.26	−2.00	−7.82	−2.47
9.37	−8.68	−5.61	−2.17	−7.11	−9.60	−2.09	−5.50	−9.17	−1.94
9.37	−8.22	−3.73	−1.18	−7.81	−9.48	−1.44	−6.80	−7.47	−1.05
9.38	−9.27	−4.12	0.56	−8.85	−8.37	0.33	−8.59	−7.31	0.26
9.39	−9.53	−0.64	1.88	−10.31	−4.46	2.07	−9.06	−6.00	1.46
9.39	−6.32	−5.18	1.65	−8.64	−6.41	1.35	−7.25	−6.45	0.52
9.40	−4.66	−4.82	1.34	−5.11	−4.21	0.88	−5.91	−3.95	−0.20
9.40	−3.78	−8.01	0.61	−2.90	−2.89	0.48	−1.80	−3.46	−0.05
9.41	−2.09	−7.56	−0.66	0.74	−1.37	−0.57	3.81	−0.06	−0.56
9.42	−1.06	−6.14	−1.85	0.82	−1.04	−2.52	3.64	0.57	−2.39
9.42	−0.95	−2.20	−0.96	0.85	2.32	−1.32	3.06	2.04	−0.66
9.43	0.91	−2.14	−0.91	0.81	−0.23	−1.42	4.19	−1.42	−0.49
9.43	1.63	−0.93	−1.23	0.45	−0.84	−1.68	2.51	−1.11	−0.51
9.44	3.86	−4.51	−0.60	−0.09	−3.11	−1.71	0.61	−2.88	−0.51
9.45	4.08	−6.84	−0.02	1.39	−5.48	−0.42	−0.73	−4.13	0.71
9.45	6.87	−5.96	−1.21	3.00	−6.07	−1.50	0.12	−4.35	−0.62
9.46	4.93	−5.94	−1.23	1.63	−5.82	−1.22	−1.89	−4.25	−0.52
9.46	2.50	−4.31	−1.47	0.00	−3.81	−1.58	−2.00	−4.68	−1.46
9.47	1.75	−0.87	−0.93	−1.14	−1.85	−1.04	−3.25	−4.81	−0.98
9.47	1.32	−4.30	−0.69	−1.69	−2.81	−1.74	−3.18	−6.11	−1.61
9.48	−3.34	−4.38	−0.28	−4.46	−0.56	−1.47	−4.78	−4.72	−1.57
9.49	−2.52	−5.45	−0.49	−0.49	−1.53	−1.67	−1.17	−4.42	−1.84
9.49	0.37	−8.01	−0.08	0.82	−4.59	−0.89	−1.65	−6.28	−0.97
9.50	−2.60	−6.47	−0.90	−0.43	−3.13	−1.11	−2.73	−3.41	−0.98
9.50	−4.56	−4.78	−0.79	−2.57	−2.13	−0.61	−3.78	−2.76	−0.71
9.51	−4.39	−4.64	−1.17	−1.59	−4.69	−0.82	−2.54	−3.71	−0.76
9.52	−6.45	−4.66	−1.42	−6.11	−4.81	−0.95	−6.51	−4.31	−0.48
9.52	−7.72	−5.93	−1.10	−6.53	−6.20	−0.42	−6.55	−5.79	−0.34
9.53	−7.57	−6.18	−1.21	−6.68	−8.14	−0.75	−6.51	−7.72	−0.88
9.53	−6.47	−8.43	−1.66	−5.65	−10.16	−1.17	−5.45	−9.75	−1.22
9.54	−5.34	−11.37	−1.04	−4.87	−12.30	−0.66	−4.97	−12.34	−0.80
9.55	−5.74	−10.20	−0.30	−5.03	−12.15	−0.90	−4.66	−13.29	−0.93
9.55	−6.15	−9.83	−0.44	−5.65	−11.19	−1.06	−5.52	−11.68	−0.89
9.56	−6.04	−10.80	−0.45	−5.99	−10.99	−0.85	−5.65	−11.54	−0.88
9.56	−7.47	−6.62	−0.07	−7.41	−7.15	−0.33	−7.56	−6.49	−0.28
9.57	−8.46	−4.24	−0.26	−8.59	−4.10	−0.28	−8.83	−3.16	−0.13
9.58	−6.96	−7.65	−0.02	−7.39	−6.63	0.40	−7.43	−6.13	−0.09
9.58	−5.63	−5.99	−0.67	−4.23	−4.86	−0.16	−4.30	−4.81	−0.68
9.59	−5.57	−6.46	−0.30	−3.87	−6.04	−0.03	−3.95	−6.49	−0.33
9.59	−5.97	−6.48	−0.25	−3.70	−7.12	0.09	−3.06	−9.45	−0.23
10.00	−7.52	−2.62	0.08	−4.77	−3.06	0.39	−3.95	−5.45	−0.11

[a]Time: 0932–1000 GMT, June 2, 1988. Location: Chung Li, Taiwan.

arrays are all 17 deg from zenith vertically, one facing toward the north, the second toward the east, and the other facing the west. The radial velocities of the winds observed from the three arrays are, then, fitted into Eq. (1), and the three-dimensional wind speeds are computed. We also can combine the three arrays in the same direction to increase the power of radar beams and make them face 17 deg from the zenith vertically. These combined beams swing from north to west, and then to south and east continually. The method of analysis is similar to one described earlier.

The time-independent three-dimensional wind profiles for heights from 70 to 95 km before and during the time periods of the tropical storm and Typhoon Susan activities were observed from the vhf radar. The observed wind radial velocities can be decomposed to horizontal and vertical components through the computation of Eq. (1). Tables 1 and 2 show the three-dimensional wind speeds observed from the vhf radar at the selected heights of 76.4, 79.5, and 92.2 km from 0747 to 0815 GMT, May 27, 1988 (tropical storm); and at the other selected heights of 76.4, 82.7, and 85.9 km from 0932 to 1000 GMT, June 2, 1988 (Typhoon Susan), respectively. Figure 4 shows the horizontal wind profile (with maximum wind corresponding to 8 m/s, indicated with the longest arrow), which is computed from the horizontal component of the radial wind velocities observed from the radar. Figure 5 illustrates the vertical wind profile (solid line denotes the updraft, and the dashed line denotes the downdraft), which is computed from the vertical component of the radial velocities observed from the vhf radar during the time periods of tropical storm activity. Figure 6 shows another horizontal wind profile (with maximum wind corresponding to 14 m/s, indicated with the longest arrow). Figure 7 describes the vertical wind profile (solid line denotes the updraft, and the dashed line denotes the downdraft), which is computed from the vertical component

of the radial velocities observed from the vhf radar during the time periods of Typhoon Susan activity. A description of the symbols for the vertical wind profiles are included in the figure legends.

C. Detection of Gravity Waves

The gravity-wave motion field is most evident in the radial velocities, and also can be observed in the backscattered power and spectral width. Frequency, horizontal wavelength, vertical wavelength, and phase velocity of gravity waves can be determined from the Fourier power spectrum analysis of the horizontal and vertical wind velocities which are decomposed from the radial velocities deduced from the multiple beams of the vhf radar and their cross-correlation analysis.[14,15,31]

Gravity waves associated with tornado activity[18,28,37] and a hurricane[24,25] have been observed. By using a ray-tracing technique, Hung et al.[26,28] have shown that the enhanced convection-initiated gravity waves associated with severe storms were generated by thunderheads embedded in a squall line and/or isolated cloud with intense convection.

High wind shear, flows across topographical barriers, and convectively unstable flows are believed to be the major causes of the excitation of gravity waves. Of the three dominant cases, convection as a source of gravity waves is the least understood. In the case studied here, wave-like disturbances were observed in the three-dimensional wind data that were decomposed from the radial velocities deduced from the three arrays of the vhf radar, all 17 deg from zenith. The first faced toward the north, the second toward the east, and the third toward the north. Detailed descriptions of the data analysis techniques for the deduction of gravity waves are given by Hung et al.[22,30] and Hung and Smith.[29]

Tables 3 and 4 show the characteristics of the gravity waves detected at the selected heights of 71.1, 75.9, 78.3, 90.3, and 92.7 km during the time period of tropical storm activity (May 27, 1988), and at the selected heights of 75.9, 78.3, 80.7, 83.1, and 85.5 km during the time period of Typhoon Susan activity (June 2, 1988), respectively.

Location of the wave sources of gravity-wave excitation can be determined from the ray-tracing computation. Wave frequency, horizontal and vertical wavelengths, and the propagation direction of gravity waves, in conjunction with the wind velocities, which are all deduced from the vhf data, have been used in the ray-tracing computation. Detailed descriptions of the ray-tracing technique for the determination of the location of the wave source are given by Hung and Kuo[24] and Hung et al.[22,26,27] Results from the ray tracing show that the major gravity waves detected on May 27, 1988, were potentially from the tropical storm located in the South China Sea; and the major gravity waves observed on June 2, 1988, were from Typhoon Susan located southwest of Taiwan. Comparisons between Tables 3 and 4 show that the wave period of gravity-waves associated with tropical storms were in the range of 5.5–8.0 min, and those associated with Typhoon Susan were in the range of 7.0–9.5 min. The horizontal wavelength for gravity waves associated with tropical storms were in the range of 9.4–19.9 km, and that associated with Typhoon Susan were in the range of 14.7–38.3 km.

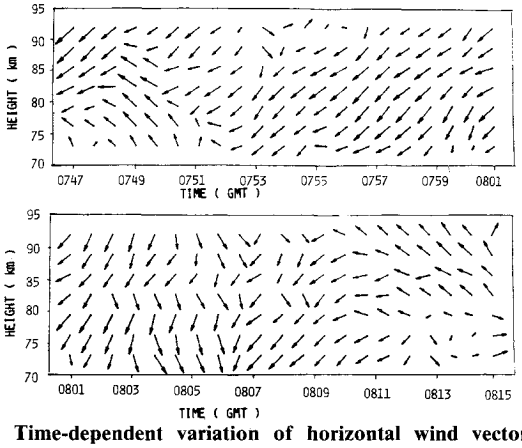

Fig. 4 Time-dependent variation of horizontal wind vectors for heights from 70 to 95 km, during the tropical storm time period of 0747 to 0815 GMT, May 27, 1988, observed from the vhf radar at Chung Li, Taiwan. The maximum wind velocity is indicated with the longest arrow corresponding to 8 m/s.

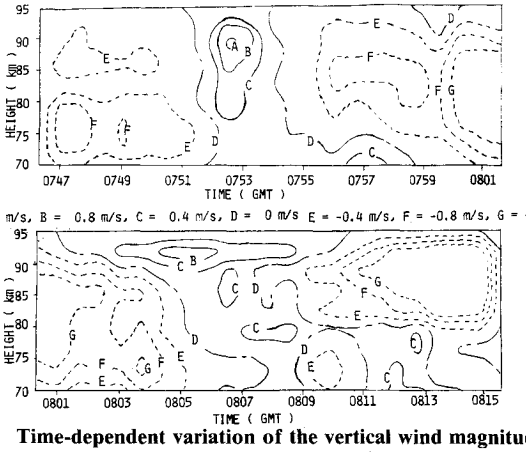

Fig. 5 Time-dependent variation of the vertical wind magnitude for the heights of 70–95 km, during the tropical storm time period of 0747–0815 GMT, May 27, 1988, observed from the vhf radar at Chung Li, Taiwan.

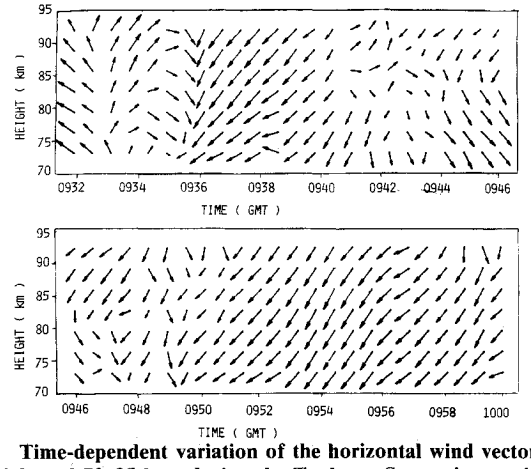

Fig. 6 Time-dependent variation of the horizontal wind vectors for the heights of 70–95 km, during the Typhoon Susan time period of 0932–1000 GMT, June 2, 1988, observed from the vhf radar at Chung Li, Taiwan. The maximum wind velocity is indicated with the longest arros corresponding to 14 m/s.

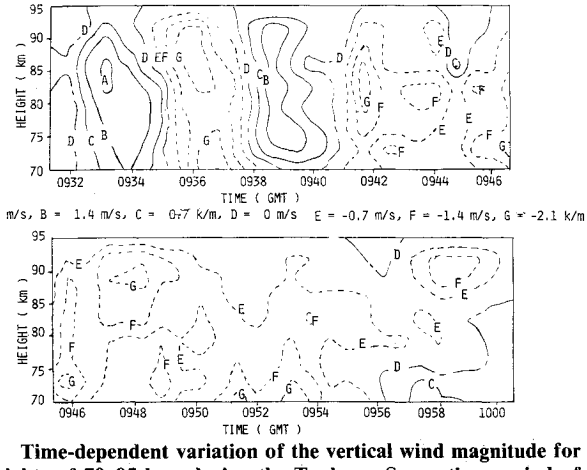

Fig. 7 Time-dependent variation of the vertical wind magnitude for the heights of 70–95 km, during the Typhoon Susan time period of 0932–1000 GMT, June 2, 1988, observed from the vhf radar at Chung Li, Taiwan.

Table 3 Characteristics of major gravity waves observed via vhf radar during tropical storm activity[a]

Height, km	Wave period, min	Wavelength, km		Horizontal direction of propagation (clockwise from north)	Phase velocity, m/s	
		Horizontal	Vertical		Horizontal	Vertical
71.1	5.7	12.0	9.6	30	35	28
75.9	6.8	9.4	7.3	28	23	18
78.3	7.2	19.2	11.7	31	44	27
90.3	8.0	19.9	13.0	26	42	27
92.7	5.5	12.8	9.2	21	39	28

[a] Time: 0747–0815 GMT, May 27, 1988. Location: Chung Li, Taiwan.

Table 4 Characteristics of major gravity waves observed via vhf radar during typhoon Susan passage[a]

Height, km	Wave period, min	Wavelength, km		Horizontal direction of propagation (clockwise from north)	Phase velocity, m/s	
		Horizontal	Vertical		Horizontal	Vertical
75.9	7.0	14.7	10.5	18	35	25
78.3	7.4	27.2	16.9	18	62	38
80.7	7.8	24.4	17.8	24	52	38
83.1	8.8	38.3	21.6	31	73	41
85.5	9.5	30.2	16.0	22	53	28

[a]Time: 0932–1000 GMT, June 2, 1988. Location: Chung Li, Taiwan.

D. Atmospheric Density Perturbation Caused by the Propagation of Gravity Waves

It is believed that density perturbations are greatly affected by the propagation of gravity waves. Gravity waves play a particularly important role in affecting the density perturbations in the middle atmosphere. The structure of the short-term middle and upper atmospheric density changes is a key element needed for space vehicle design purposes. Projects such as Space Shuttle, National Aerospace Plane, Shuttle II, Aeroassisted Flight Experiment (AFE), Aerobraking Orbital Transfer Vehicle (AOTV), and space station will benefit from such studies. In particular, the upper atmospheric density perturbation affects the drag and the lift forces of spacecrafts and space system that, in turn, affects the design of propulsion, guidance, control, and stability systems of the space vehicle.

Let us consider acoustic-gravity wave propagating in the terrestrial atmosphere, which is assumed to be compressible, nonrotating, and adiabatic. The assumption of a nonrotating terrestrial atmosphere is based on the fact that the wave period of acoustic-gravity waves is less than an hour which is much less that the rotating period of the Earth. The assumption of an adiabatic atmosphere is because the velocity of heat conduction of an terrestrial atmosphere, from the surface to a height of ~300 km, is much less than the speed of sound. Detailed derivation of atmospheric density perturbations caused by the propagation of acoustic-gravity waves is illustrated in Hung et al.[25] The expression for an atmospheric density perturbation can be shown as follows[25]:

$$\frac{\rho'}{\rho_0} = -\left\{1+\frac{(N/\omega)^2-(g\Gamma_d/T_0\omega^2)}{\{[(V_p)_H v_H\cos\theta_p/2(v_p)_v v_v]-1\}}\right\}^{-1} \times\left\{(\gamma-1)\left[\frac{v_H}{(v_p)_H}\cos\theta_p+\frac{v_v}{(v_p)_v}\right]+\frac{\gamma(v_p)_H v_H\cos\theta_p}{2C^2}\right\} \quad (2)$$

Here ρ' denotes the perturbed quantity of the atmospheric density; ρ_0, the equilibrium quantity of the atmospheric density; g, the gravitational acceleration; γ, the ratio of the constant pressure specific heat to the constant volume specific heat; T_0, the equilibrium quantity of the atmospheric temperature; C, the speed of sound; v_H, the horizontal wind velocity; $(v_p)_H$, the horizontal phase velocity of the gravity waves; v_v, the vertical wind velocity; $(v_p)_v$, the vertical phase velocity of the gravity waves; and θ_p, the angle between the horizontal phase velocity of the gravity waves and the horizontal wind velocity.

The Brunt-Vaisalla frequency N is defined by

$$N^2=\frac{g}{T_0}\left[\Gamma_d+\frac{dT_0}{dz}\right] \quad (3)$$

where

$$\Gamma_d=\frac{g}{C_p} \quad (4)$$

is the adiabatic lapse rate, and C_p denotes the constant pressure specific heat.

Horizontal and vertical wind velocities can be directly observed from the signal returns of the vhf radar, whereas the gravity-wave characteristics of horizontal and vertical phase velocities and wave frequency can be computed from power spectral and cross-correlation analysis of the vhf backscattered echo. Thus, one can use Eqs. (2–4) to compute density perturbations caused by the propagation of gravity waves.

A decrease of received power as a function of the height above the ground is experienced by the vhf radar.[1] A general feature to be noted is that the received signal above the altitude of 20 km is particularly weak. However, such vhf radars are often capable of obtaining high-quality data from heights above 70 km in the daytime, especially summer, because of electron scattering. In particular, the observation of time-dependent wind profiles from vhf radar are quite possible in the mesosphere above the 70-m height during the time period of peak solar cycle and strong flare activity.

In this study, atmospheric density perturbations at mesospheric heights were calculated from Eq. (2) using the wind profiles and the characteristics of gravity waves observed by the vhf radar during the time period of the tropical storm and Typhoon Susan activities. Figures 8 and 9 show the perturbation of atmospheric density at the selected heights of 71.1, 75.9, 78.3, 90.3, and 92.7 km during the time period of

0747–0815 GMT, May 27, 1988 (tropical storm activity); and at the selected heights of 75.9, 78.3, 80.7, 83.1, and 85.5 km during the time period of 0932–1000 GMT, June 2, 1988 (Typhoon Susan activity), respectively. The following results can be concluded based on Figs. 8 and 9: 1) There were time-dependent wave-like disturbances shown in the mesospheric atmospheric density perturbations in which the phase and time relationship showed that the waves were propagating upward from the lower atmosphere. 2) The maximum amplitude of the density perturbations caused by the gravity waves associated with Typhoon Susan was ±15%, which was greater than that caused by the gravity waves associated with tropical storms (which was ±12%). 3) Longer wave periods of density perturbations were observed for waves associated with the typhoon (greater-scale energy sources) than that for waves associated with the tropical storm (lower-scale energy sources).

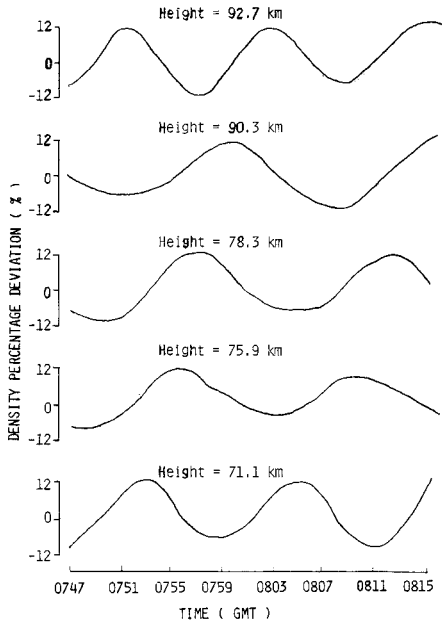

Fig. 8 Mesospheric density perturbations caused by the propagation of gravity waves associated with tropical storms at selected heights, during the time period of 0747–0815 GMT, May 27, 1988, observed from the vhf radar at Chung Li, Taiwan.

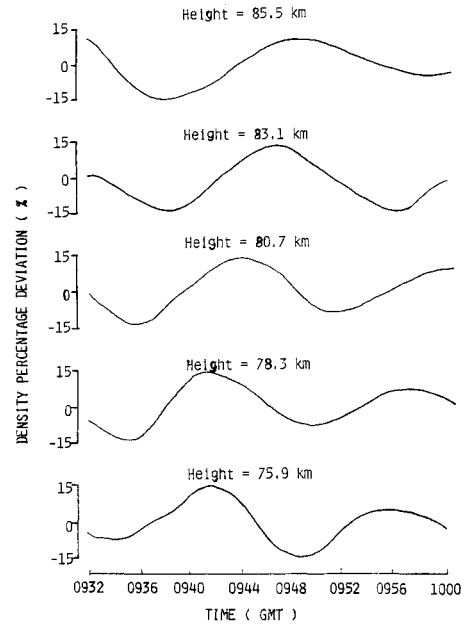

Fig. 9 Mesospheric density perturbations caused by the propagation of gravity waves associated with Typhoon Susan at selected heights, during the time period of 0932–1000 GMT, June 2, 1988, observed from the vhf radar at Chung Li, Taiwan.

III. HF Doppler Array Observation of Thermospheric Density Disturbance During the Time Period of Typhoon Activity

A. Meteorological Background

At 0000 GMT, August 27, 1987, Typhoon Dinah was located at the Pacific Ocean, 900 km southeast of Taiwan. Figure 10 shows a satellite infrared imagery of Typhoon Dinah at 0000 GMT, August 27, 1987. Figure 11 shows the storm path of Typhoon Dinah. At the moment of satellite imagery shown in Fig. 10, this storm moved in a northwest direction with a central storm pressure of 925 mb. Figure 12a shows a 850-mb weather map at 0000 GMT, August 27, 1987. This map shows that the area of low pressure covered the whole areas of North China and Manchuria. A cold front then developed from this area of low pressure and extended southwest through Central China. On the other hand, the Tibet Plateau was also covered by the area of low pressure (see Figs. 10 and 12 for the comparison). The 300-mb weather map also shows that there were divergent flowfields located at Central and South China.

Figure 12b shows a 850-mb weather map at 0000 GMT, August 28, 1987. At this moment, the typhoon moved to 700 km southeast of Taiwan, and turned toward the north in a northwest direction with a central storm presure of 920 mb. A low-presure belt extended from the Tibet Plateau through Central and North China, passing over the Korean Peninsula, and reaching northeast Japan. There was also a cold front that

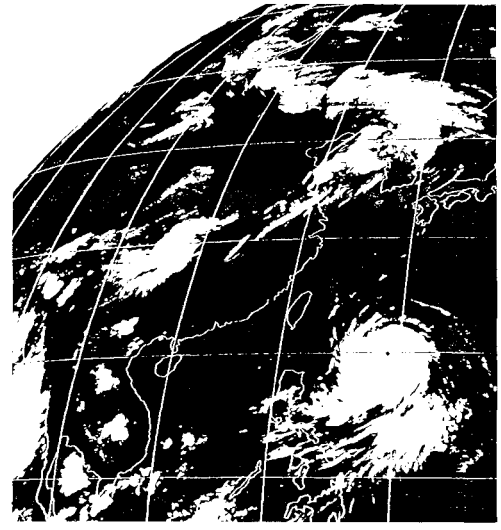

Fig. 10 Satellite infrared imagery of Typhoon Dinah at 0000 GMT, August 27, 1987.

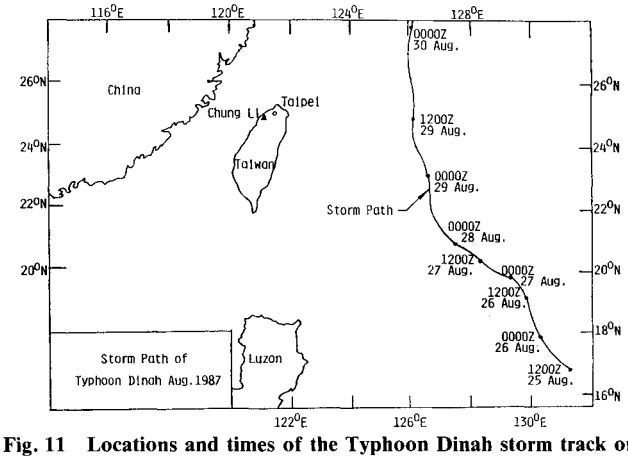

Fig. 11 Locations and times of the Typhoon Dinah storm track on August 25–30, 1987.

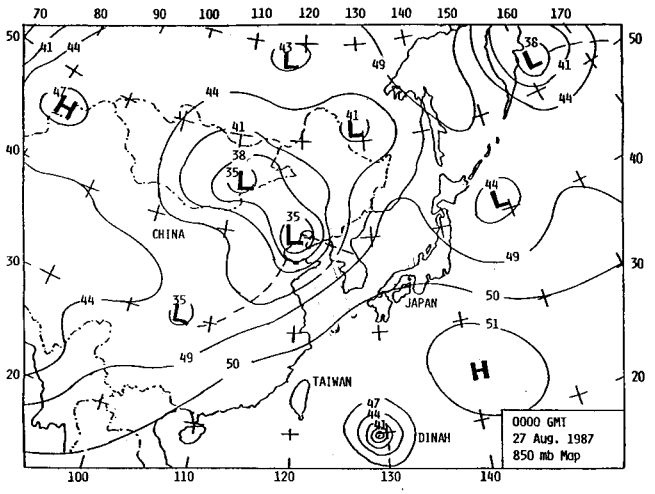

Fig. 12a 850-mb weather map of the Far East area at 0000 GMT, August 27, 1987.

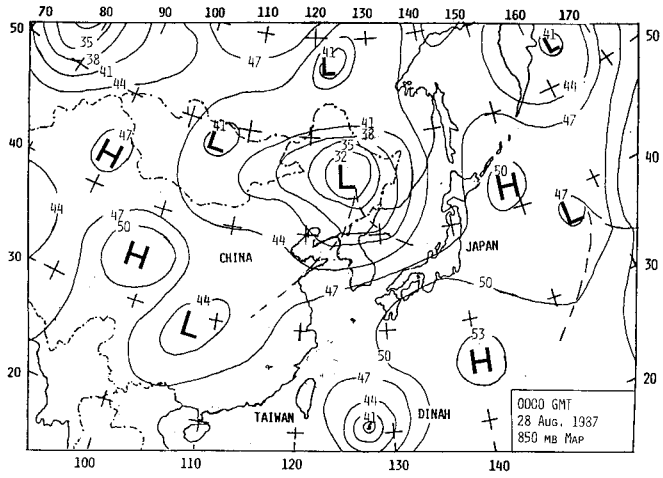

Fig. 12b 850-mb weather map of the Far East area at 0000 GMT, August 28, 1987.

extended from North China in a southwesterly direction to Central China and moved in a southeasterly direction. The 300-mb weather map indicates that there were divergent flow-fields located in Central and South China.

Knowing these background conditions, it is possible to anticipate the observation of gravity waves induced by strong convection in the troposphere and propogated to the thermosphere.[28,29]

B. Detection of Gravity Waves and Determination of Wind Speed and Density Perturbations

A high-frequency (hf) Doppler sounder array installed at the National Central University (NCU), Chung Li, Taiwan, was used to study lower thermospheric density fluctuations caused by a violent convective storm—Typhoon Dinah. The NCU hf Doppler sounder has three transmitters located at Iilan (24.7°N, 121.7°E), Hualien (24.0°N, 121.6°E), and Sun Moon Lake (23.8°N, 120.9°E). The receiver of the array is located at Chung Li (25°N), 121°E). The geographical description of NCU hf Doppler sounder array is illustrated in Fig. 13. The nominal frequency of the NCU hf Doppler is 3.985 MHz. Another two sets of hf Doppler sounder arrays also installed in the same location, operated by the Commission General of Telecommunication (CGL), Ministry of Communication of Taiwan, are used in conjunction with the NCU hf Doppler for the data analysis. Two nominal frequencies adopted by the CGL hf Doppler are 5.2 and 7.8 MHz.

During periods of severe weather activity, TIDs are observed in high-frequency CW Doppler records. The data from

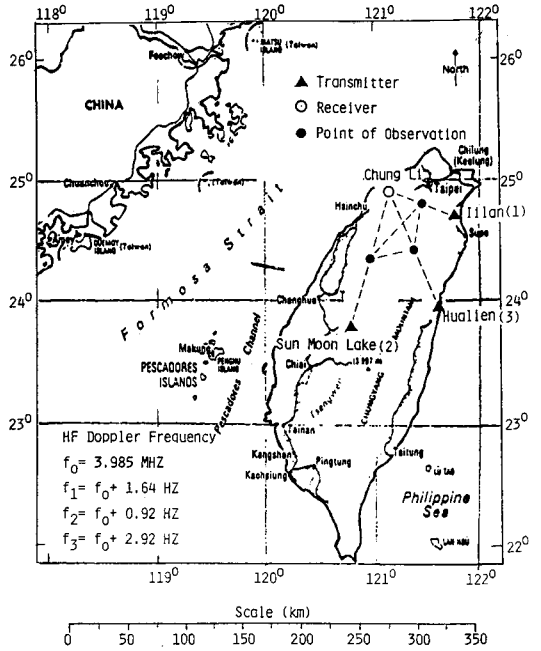

Fig. 13 Geographical location of hf Doppler sounder array operated by the National Central University, Chung Li, Taiwan.

the Doppler sounder array are subjected to a power spectral density analysis to obtain wave periods of these Doppler fluctuations while the direction of the propagation and the phase velocity of the waves are obtained from a cross-correlation analysis.[24,37] Group ray-tracing computations using the best available data on the thermodynamic properties of the atmosphere are used in determining the locations of the sources of the waves. A detailed description of the observation system, the data processing techniques, wind data, and atmospheric models used in ray-tracing computation are given in Hung and Smith,[23] Hung et al.,[22] Hung and Kuo.[24]

For the gravity-wave study, the probable errors in the determination of the azimuthal angle of the wave arrival and the ray-tracing computation have been discussed by Hung et al.,[22] Hung and Smith,[23] and Hung and Kuo.[24]

Gravity waves associated with tornado activity[22] and hurricanes/typhoons[24,25] have been observed. By using a ray-tracing technique, Hung et al.[24-26,34] have shown that the enhanced econvection-initiated gravity waves associated with severe storms and hurricane/typhoons were generated by thunderheads embedded in a squall line, isolated cloud, and/or wall clouds with intense convection.

High wind shear, flows across topographical barriers, and convectively unstable flows are believed to be the major causes of the excitation of gravity wavs. Of the three dominant cases, convection as a source of gravity waves is the least understood. In the case studied here, TID were observed from the high hf Doppler reflected from F-region ionospheres for this stormy day.

Horizontal wind velocity in the direction of gravity-wave propagation can be observed in hf CW Doppler records. From the Boussinesq approximation, horizontal phase velocity of gravity waves is much less than the speed of sound, which is usually the case for the so-called medium scale TID, whose horizontal phase velocity generally does not exceed 250 m/s in the F-region ionosphere. Under these conditions, the dispersion relation of acoustic-gravity waves becomes[38]

$$(\omega/k_H) \equiv (v_p)_H = (N\lambda/2\pi) + v_H \tag{5}$$

Here, ω denotes the frequency of gravity waves; k_H, the horizontal wave number of gravity waves; $(v_p)_H$, the horizontal phase velocity of gravity waves; v_H, the horizontal wind velocity in the direction of gravity-wave propagation; N, the Brunt-Vaisalla frequency; and λ, the wavelength of gravity waves,

which is given by

$$\lambda = 2\pi/(k_H^2 + k_v^2)^{1/2} \quad (6)$$

Here, k_v denotes the vertical wave number of gravity waves.

Following the data analysis procedures given by Crowley et al.,[38] one can determine the horizontal wind profile in the direction of gravity-wave propagation, as shown in Eq. (5).

Three sets of hf Doppler sounder arrays have been used to observe thermospheric disturbances during the time period of Typhoon Dinah. In this paper, 7 h of observations of Doppler records, from 0400–1100 GMT, August 28, 1987, were used to detect gravity-wave disturbances at three different heights of the thermosphere. The ionospheric reflection heights of the hf Doppler arrays were measured from ionosound which was also available at Chung Li, Taiwan. The time-dependent hf radio wave reflection heights from F-region ionosphere during the time period of 0400–0730 GMT are shown in the top lines of Fig. 14, whereas that of the time period of 0730–1100 GMT are illustrated in the similar top lines of Fig. 15. Ionospheric reflection height (1) corresponds to hf Doppler sounder with the nominal frequency 7.8 MHz; reflection height (2), the nominal frequency 5.2 MHz; and reflection height (3), the nominal frequency 3.985 MHz.

Gravity waves at three reflection heights of ionosphere were detected from hf Doppler records.[22-24] Typical characteristics of gravity waves detected at height (1) are illustrated in Table 5; at height (2) in Table 6; and at height (3) in Table 7. These figures show wave period, wavelength, phase velocity, and propagation direction of gravity waves measured clockwise from geomagnetic north for typical gravity waves detected at selected time period of observations. Most of the gravity waves detected during the time period of 0400–1100 GMT, August 28, 1987, were the mesoscale rather than the large-scale gravity waves. In other words, the gravity waves originated from severe convective motion rather than being associated with aurora activity in which three hourly indices of the K_p index, on this particular day, were either 2 or 3, which are too low to excite large-scale gravity waves during the time period of wave observation.[5,22]

Calculation of atmospheric density perturbations at thermospheric heights based on the method described by Hung et al.[25] are the summation of Fourier components of each gravity wave detected contributing to the excitation of density perturbations. Among all of the gravity waves detected at the time of interest, there is a major gravity wave that dominates the contribution of the excitation of atmospheric density perturbations. Phase velocity (both magnitude and direction) of these major gravity waves detected during the time period of 0400–0730 are illustrated in Fig. 16, whereas that of the major gravity waves detected during the time period of 0730–1100 are shown in Fig. 17.

In Figs. 16 and 17, at each of the heights of reflection from ionosphere, line (C) shows magnitudes (Arabic numbers representing meters/seconds) and direction (arrow) of the major gravity waves with sources from the southeast; line (D) illustrates the major gravity waves with sources from the northwest and northeast directions observed at the time (in GMT) illustrated at the bottom of each figure. Ray-tracing computation shows that the gravity waves with sources from the southeast were excited by the wall clouds of Typhoon Dinah, and those with sources from the northeast, by the convective cloud band of a cold front from the Korean Peninsula.

Component of horizontal wind profile parallel with the direction of gravity-wave propagation at three different thermospheric heights observed from the hf Doppler sounding can be determined from the data analysis procedures given by Crowley et al.[38] Phase velocity of the major gravity waves during the time period of observation is illustrated in Figs. 16 and 17. One can thus compute the component of horizontal wind profile parallel with the direction of gravity-wave propagation.[38] Tables 5–7 shows that there were several gravity waves detected in the same time during the time period of interest. For each gravity wave, one can compute the component of horizontal wind profile parallel with the direction of the wave propagation. A resultant profile of wind velocity,

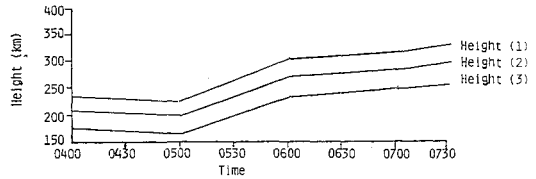

a) Reflection heights of hf radio waves

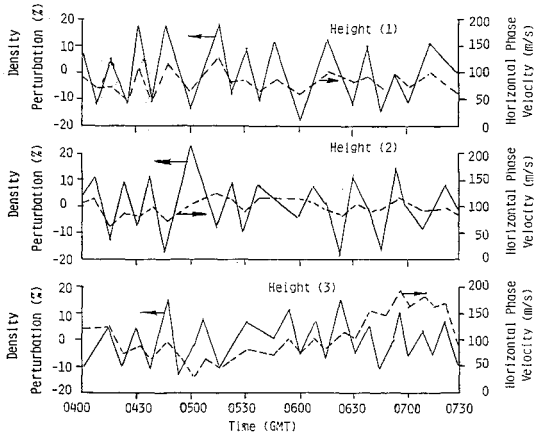

b) Density perturbation and magnitude of horizontal phase velocity of gravity waves

Fig. 14 Time-dependent hf radio wave reflection heights and density perturbations during the time period of 0400–0730 GMT, August, 28, 1987: a) (1) = nominal frequency 7.8 MHz, (2) = nominal frequency 5.2 MHz, and (3) = nominal frequency 3.985 MHz; and b) solid line = density perturbations, hidden line = horizontal phase velocity of major gravity waves, m/s.

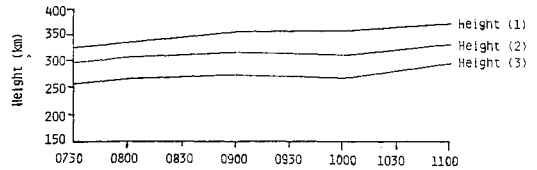

a) Reflection heights of hf radio waves

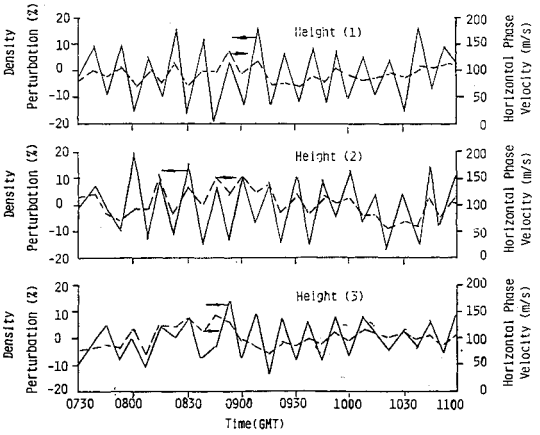

b) Density perturbation and magnitude of horizontal phase velocity of gravity waves

Fig. 15 Time-dependent hf radio wave reflection heights and density perturbations during the time period of 0730–1100 GMT, August 28, 1987; a) (1) = nominal frequency 7.8 MHz, (2) = nominal frequency 5.2 MHz, and (3) = nominal frequency 3.985 MHz; and b) solid line = density perturbations, hidden line = horizontal phase velocity of major gravity waves, m/s.

Table 5 Characteristics of gravity waves and wind observed at thermospheric heights[a]

		Gravity wave				Wind	
Time, GMT	Height, km	Wave period, min	Wavelength, km	Phase velocity, m/s	Propagation direction (degrees from north)	Velocity, m/s	Direction (degrees from north)
05:21	184	13.6	126.7	155.2	166.6	102	242
		16.0	63.8	66.5	142.3		
		17.1	199.7	195.1	48.2		
		20.2	102.1	83.9	181.1		
		28.8	106.6	61.6	83.3		
07:03	250	16.8	190.8	189.2	103.3	85	256
		27.7	176.9	123.1	204.9		
08:16	272	16.0	118.6	123.6	113.2	104	261
		19.7	62.1	62.4	133.2		
08:20	272	15.4	146.5	157.9	137.8	129	238
		21.1	76.0	60.1	161.0		
08:59	279	15.2	204.3	224.0	152.1	64	271
		20.0	78.3	65.2	150.0		
		21.6	71.4	55.1	145.2		
09:20	278	15.2	90.4	96.1	154.7	149	248
		19.7	101.8	86.1	161.6		
		21.8	60.4	46.1	141.6		
		22.9	60.7	44.1	136.8		

[a]Location: Chung Li, Taiwan. Time: August 28, 1987. HF Doppler sounder: 3.9 MHz.

Table 6 Characteristics of gravity waves and wind observed at thermospheric heights[a]

		Gravity wave				Wind	
Time, GMT	Height, km	Wave period, min	Wavelength, km	Phase velocity, m/s	Propagation direction (degrees from north)	Velocity, m/s	Direction (degrees from north)
04:30	205	24.3	143.4	98.5	181.5	108	299
		26.9	92.2	57.1	50.9		
		30.1	91.9	50.8	76.9		
05:21	219	22.9	143.6	104.4	172.3	51	269
		24.5	143.0	97.2	176.1		
05:59	264	20.0	123.4	120.8	157.0	70	259
		24.5	83.2	56.5	125.4		
		30.9	116.3	55.5	159.6		
07:42	292	19.4	104.5	120.3	120.8	84	265
		22.1	75.2	56.8	91.5		
07:59	298	18.1	66.9	61.5	148.0	67	294
		19.4	57.2	48.9	157.0		
		22.6	115.3	84.8	105.2		
		26.4	60.7	38.3	106.2		
		42.1	44.7	17.7	153.5		
08:37	315	23.2	97.1	69.8	167.1	53	248
		24.2	188.6	129.5	17.9		
		25.1	162.1	107.8	184.0		
09:54	315	15.7	101.7	107.8	124.0	76	268
		23.2	105.8	76.0	100.6		
		25.3	94.6	62.2	121.7		
10:11	313	16.0	141.0	146.9	118.7	135	248
		18.1	41.3	37.9	179.5		
		23.7	54.2	38.9	157.0		
		24.0	75.8	52.7	159.5		
		25.1	77.1	51.2	152.1		
10:37	324	17.1	93.5	91.2	65.5	63	275
		21.8	52.4	40.0	114.6		
		25.1	84.3	56.2	134.9		
10:45	327	21.1	55.5	43.9	125.7	141	280
		22.6	46.9	34.4	148.6		
		23.4	45.5	32.3	149.1		
		24.2	175.2	120.3	151.1		

[a]Location: Chung Li, Taiwan. Time: August 23, 1987. HF Doppler sounder: 5.2 MHz.

Table 7 Characteristics of gravity waves and wind observed at thermospheric heights[a]

		Gravity wave				Wind	
Time, GMT	Height, km	Wave period, min	Wavelength, km	Phase velocity, m/s	Propagation direction (degrees from north)	Velocity, m/s	Direction (degrees from north)
04:17	233	22.4	97.9	72.9	89.9	117	285
		23.2	98.5	70.8	93.6		
		24.8	233.3	156.8	89.4		
		32.5	154.4	79.1	97.0		
06:04	300	19.5	113.5	97.2	176.1	105	265
		20.0	116.6	97.2	176.1		
		24.8	145.3	97.6	32.2		
		27.7	139.3	83.7	57.6		
07:21	320	16.0	48.1	50.1	154.5	91	242
		22.4	74.6	55.5	159.7		
		23.7	80.9	56.8	151.5		
		24.8	65.4	43.9	125.8		
07:50	330	15.7	49.3	52.2	164.6	70	258
		16.5	70.7	71.3	143.1		
		17.1	72.5	70.8	160.4		
		25.6	45.3	29.5	113.6		
08:29	334	17.1	85.7	83.7	16.4		
		20.0	36.3	30.2	34.1		
		21.3	42.1	32.9	20.9		
		24.8	113.7	76.4	51.9		
		59.2	100.1	28.1	131.7		
08:46	337	24.3	78.5	53.9	42.2	123	292
		27.2	51.3	31.4	18.5		
		30.6	41.2	22.8	22.4		
		59.7	113.9	31.8	134.9		
09:33	357	15.7	87.2	92.3	28.1	136	274
		19.2	68.3	59.3	3.7		
		26.7	40.8	25.5	25.8		
		27.5	44.4	26.9	19.8		
09:50	356	16.0	73.3	76.4	111.9	147	249
		28.3	43.4	25.6	32.1		
		33.0	37.7	19.0	23.1		

[a]Location: Chung Li, Taiwan. Time: August, 28, 1987. HF Doppler sounder: 7.8 MHz.

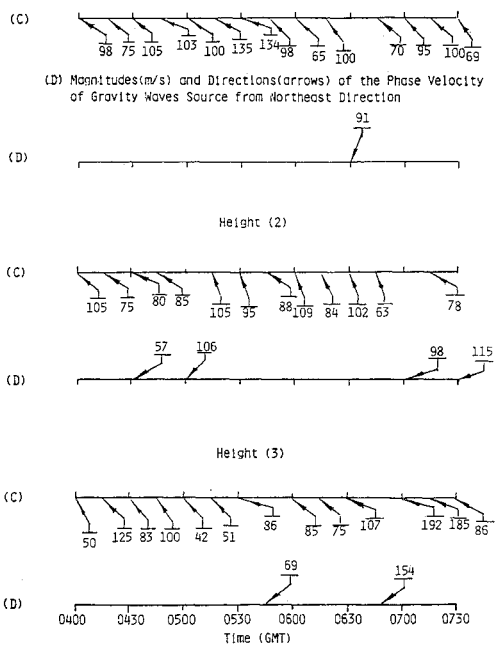

Fig. 16 Horizontal phase velocities of major gravity waves observed during the time period of period of 0400–0730 GMT, August 28, 1987: Magnitudes (m/s) and direction (arrows) of the phase velocity of major gravity waves from the southeast (c) and northeast (d).

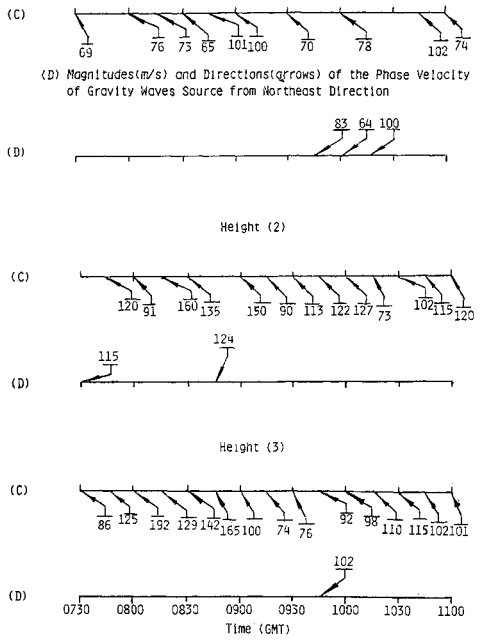

Fig. 17 Horizontal phase velocities of major gravity waves observed during the time period of 0730–1100 GMT, August 28, 1987. Magnitudes (m/s) and direction (arrows) of the phase velocity of major gravity waves from the southeast (c) and northeast (d).

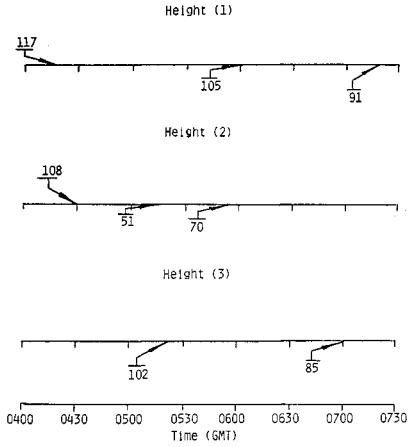

Fig. 18 Time-dependent magnitude (m/s) and direction (arrows) of the resultant horizontal wind velocity observed during the time period of 0400–0730 GMT, August 28, 1987. Time-dependent hf radio wave reflection heights (1), (2), and (3) observed from ionosonde are shown in the top lines of Fig. 14.

therefore, can be obtained based on the vector summation of two or more components of wind profiles parallel with the direction of each gravity-wave propagation. Figures 18 and 19 show the observed thermospheric wind velocity at three different reflection heights from the ionosphere during the time period of 0400–0730 GMT and 0730–1100 GMT, respectively. In these two figures, again the magnitudes of wind velocity are shown by Arabic numbers representing meters/second, and the directions of wind velocity are shown by the arrow. The resultant wind velocity computed from the components of wind velocity parallel with the typical waves detected at the selected time period of observations is also illustrated in Tables 5–7.

Let us consider acoustic-gravity waves propagating in the terrestrial atmosphere, which is assumed to be compressible, nonrotating, and adiabatic. The assumption of a nonrotating terrestrial atmosphere is based on the fact that the wave period of acoustic gravity waves is less than an hour, which is much less than the rotating period of the Earth, and the assumption of an adiabatic atmosphere is because the velocity of heat conduction of a terrestrial atmosphere from the surface to a height of about 300 km is much less than the speed of sound. Detailed derivation of atmospheric density perturbations caused by the propagation of acoustic-gravity waves is illustrated in Hung et al.[25]

In this study, atmospheric density perturbations at thermospheric heights were calculated from the method described by Hung et al.[25] through the wind profile computed from Eq. (5), which are shown in Figs. 18 and 19, and gravity waves shown in Figs. 16 and 17. Figures 14 and 15 show the atmospheric density perturbation at three different heights of thermosphere during the time period of 0400–0730 GMT, and 0730–1100 GMT, August 28, 1987, respectively. In Figs. 14b and 15b, the solid line shows the time-dependent density perturbation at three different heights of thermosphere; the hidden line illustrates the horizontal phase velocity of the major gravity waves (in meters/second). The following results can be concluded based on Figs. 14 and 15:

1) The maximum amplitude of the density perturbations caused by the gravity waves associated with Typhoon Dinah was ±20%.

2) The time-dependent atmospheric density perturbations were in phase with the amplitude of the variation of the horizontal phase velocity of the major gravity waves.

IV. Discussion and Conclusion

The vhf radar and hf Doppler array systems located at the subtropical area of Taiwan have been used to observe the atmospheric parameters from the troposphere, the middle atmosphere, and the thermosphere. A special event of atmospheric disturbances caused by the propagation of gravity waves excited by the enhanced convective cloud bands of Typhoon Susan, Typhoon Dinah, and tropical storms were investigated.

From the backscattered echo power and the Doppler spectral width of the signal returns from the vhf radar, we have determined the three-dimensional wind velocities at different heights. With fast algorithms and computers, this could be done in real time from the troposphere to middle atmospheric heights.

Frequency, horizontal wavelength, vertical wavelength, and phase velocity of the gravity waves have been determined from the Fourier power spectral analysis of the horizontal and vertical wind velocities from the multiple beams of the vhf radar and their cross-correlation analysis. It is found that these gravity waves detected from the troposphere to the middle atmosphere were all excited by the convective motion associated with the cloud bands of Typhoon Susan and tropical storms based on ray-tracing computation.

Gravity waves play an extremely important role in affecting the density perturbation in the middle and upper atmospheres. The structure of the short-term middle and upper atmospheric density changes is a key element needed for space vehicle design purposes. Projects such as the Space Shuttle, National Aerospace Plane, Shuttle II, Shuttle C, Tethered Satellite, Space Telescope, AOTV, and AFE will benefit from such studies.

In general, the drag and lift forces of spacecraft and space systems are deeply affected by the upper atmospheric density perturbations. In particular, the structure of the short-term middle and upper atmospheric density changes influences greatly the design of propulsion and stability systems of the space vehicle. It is particularly interesting to mention that the large-amplitude gravity waves induced by convective storms of severe weather can produce mesospheric density perturbations that change the atmospheric drag of space systems and provide a great impact on the stability and gravity-level fluctuations of the Space Telescope, AOTV, and space stations, in particular, through the variations in the buoyancy forces.

Atmospheric density perturbations caused by the propagation of gravity waves at mesopheric heights were investigated. Results show that the maximum amplitude of the density perturbations caused by the gravity waves associated with Typhoon Susan was ±15%, which was greater than that caused by the gravity waves associated with tropical storms, which was ±12%.

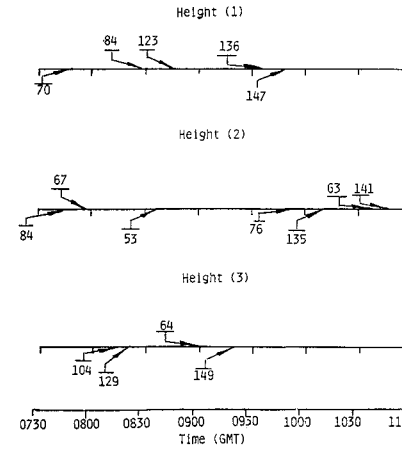

Fig. 19 Time-dependent magnitude (m/s) and direction (arrows) of the resultant horizontal wind velocity observed during the time period of 0730–1100 GMT, August 28, 1987. Time-dependent hf radio wave reflection heights (1), (2), and (3) observed from ionosonde are shown in the top lines of Fig. 15.

Gravity waves are routinely detectable in vhf radar velocity data. Large-amplitude gravity waves associated with typhoons produce greater amplitude of the density perturbations at mesospheric heights than that of the density perturbations excited by the gravity waves associated with tropical storms. In other words, it appears that the amplitude of density perturbations is proportional to the amplitude of gravity waves, which, in turn, is proportional to the momentum of the convective systems that excite gravity waves. Mesospheric gravity waves have been observed at the middle and upper (MU) atmosphere radar in Japan[16] located at midlatitude, and also vhf radar at Poker Flat, Alaska,[39-41] located at high latitude. Basically, there seems to be no difference in the characteristics of mesospheric gravity waves observed at the different latitudes, geographically, but there is a difference in the amplitude of the waves, which depends on the mechanism of the wave source originating from the different scales of convective activity. In short, the amplitude variations of the mesopheric density perturbations are very dependent on the size of momentum of the convective systems that excite gravity waves, rather than the dependency of the existence of gravity waves at the different geographical locations.

Three sets of hf Doppler sounder arrays located at the subtropical area of Taiwan have been used to observe the gravity waves, the component of horizontal wind velocity parallel with the direction of gravity-wave propagation, the resultant horizontal wind velocity, and atmospheric density perturbations at three different heights of thermosphere during the time period of Typhoon Dinah.

Atmospheric density perturbations caused by the propagation of gravity waves at thermospheric heights were investigated. Results show that the maximum amplitude of the density perturbations caused by the gravity waves associated with Typhoon Dinah was $\pm 20\%$.

In this study, we have demonstrated the use of the vhf radar and the hf Doppler sounder for remote measurement of three-dimensional winds, gravity waves, and density perturbations at mesospheric and thermospheric heights. This subtropical, low-latitude site makes the present vhf radar and hf Doppler array systems unique, and our observations especially valuable for space projects dealing with the low-latitude atmosphere.

Acknowledgments

This research was supported by NASA Grant NAG8-063, and the National Science Council of Taiwan through Grants NSC76-0202-M008-23 and MSC77-0202-M008-22. The authors would like to express their appreciation to Steve Smith of the University Space Research Association at the NASA Marshall Space Flight Center for the discussions of some technical problems. They would also like to express appreciation to Y. N. Huang and his associates at the Commission General of Telecommunication, Ministry of Communication of Taiwan, which provided hf Doppler sounder records and ionosound data during the time period of Typhoon Dinah. Part of the data processing accomplished by J. M. Liu of the University of Alabama in Huntsville is also acknowledged.

References

[1]Balsley, B. B., and Gage, K. S., "The MST Radar Technique: Potential for Middle Atmospheric Studies," *Pure and Applied Geophysics*, Vol. 118, 1980, pp. 452-493.

[2]Gage, K. S., and Balsley, B. B., "On the Scattering and Reflection Mechanisms Contributing to Clear Air Radar Echoes from the Troposphere, Stratosphere, and Mesosphere," *Radio Science*, Vol. 15, March-April, 1980, pp. 243-257.

[3]Rottger, J., "Investigations of Lower and Middle Atmosphere Dynamics Antenna Drifts Radars," *Journal of Atmospheric and Terrestrial Physics*, Vol. 43, 1981, pp. 227-292.

[4]Francis, S. H., "A Theory of Medium-Scale Traveling Ionospheric Disturbances," *Journal of Geophysical Research*, Vol. 79, 1974, pp. 5245-5260.

[5]Bertin, F., Testud, J., Kersley, L., and Ress, P. R., "The Meteorological Jet Streams as a Source of Medium Scale Gravity Waves in the Thermosphere: An Experimental Study," *Journal of Atmospheric and Terrestrial Physics*, Vol. 40, 1978, pp. 1161-1183.

[6]Davies, K., and Jones, J. E., "Ionospheric Disturbances Produced by Severe Thunderstorms," National Oceanic and Atmospheric Administration, Prof. Pap. 6, Rockville, MD, 1972, pp. 1-47.

[7]Williams, P. J. S., Van Eyken, A. P., and Bertin, F., "A Test of the Hines Dispersion Equation for Atmospheric Gravity Waves," *Journal of Atmospheric and Terrestrial Physics*, Vol. 44, 1982, pp. 573-576.

[8]Vincent, R. A., and Rottger, J., "Spaced Antenna vhf Radar Observations of Tropospheric Velocities and Irregularities," *Radio Science*, Vol. 15, 1980, pp. 319-335.

[9]Hocking, W. K., "Two Years of Continuous Measurements of Turbulence Parameters in the Upper Mesosphere and Lower Thermosphere Made with a 2-MHz Radar," *Journal of Geophysical Research*, Vol. 93, March, 1988, pp. 2475-2491.

[10]Gage, K. S., Green, J. L., and Van Zandt, T. E., "Use of Doppler Radar for the Measurement of Atmospheric Turbulence Parameters from the Intensity of Clear-Air Echoes," *Radio Science*, Vol. 15, March-April 1980, pp. 407-416.

[11]Hocking, W. K., "Observation and Measurement of Turbulence in the Middle Atmosphere," *Journal of Atmospheric and Terrestrial Physics*, Vol. 28, July 1986, pp. 655-670.

[12]Larsen, M. F., Kelley, M. C., and Gage, K. S., "Turbulence Spectra in the Upper Troposphere and Lower Stratosphere Between 2 Hours and 40 Days," *Journal of Atmospheric Science*, Vol. 39, 1982, pp. 1035-1041.

[13]Lilly, D. K., "Stratified Turbulence and the Mesoscale Variability of the Atmosphere," *Journal of Atmospheric Science*, Vol. 40, 1983, pp. 749-761.

[14]Chanin, M. L., and Houchecorne, A., "Lidar Observation of Gravity and Tidal Waves in the Middle Atmosphere," *Journal of Geophysical Research*, Vol. 86, 1981, pp. 9715-9221.

[15]Dunkerton, T. J., "Wave Transcience in a Compressible Atmosphere, Part III: The Saturation of Internal Gravity Waves in the Mesosphere," *Journal of Atmospheric Science*, Vol. 39, 1982, pp. 1042-1051.

[16]Yamamoto, M., Tsuda, T., Kato, S., Sato, T., and Fukao, S., "A Saturated Inertia Gravity Wave in the Mesosphere Observed by the Middle and Upper Atmosphere Radar," *Journal of Geophysical Research*, Vol. 92, Oct. 1987, pp. 11993-11999.

[17]Gage, K. S., and Green, J. L., "An Objective Method for the Determination of Tropopause Height from vhf Radar Observations," *Journal of Applied Meteorology*, Vol. 21, 1982, pp. 1150-1154.

[18]Larsen, M. F., and Rottger, J., "Comparison of Tropopause Height and Frontal Boundary Locations Based on Radar and Radiosonde Data," *Geophysical Research Letters*, Vol. 10, 1983, pp. 325-328.

[19]Rottger, J., "VHF Radar Observations of a Frontal Passage," *Journal of Applied Meteorology*, Vol. 18, 1979, pp. 85-91.

[20]Green, J. L., and Gage, K. S., "Observations of Stable Layers in the Troposphere and Stratosphere Using VHF Radar," *Radio Science*, Vol. 15, 1980, pp. 395-406.

[21]Rastogi, P. K., and Rottger, J., "VHF Radar Observations of Coherent Reflections in the Vicinity of the Tropopause," *Journal of Atmospheric and Terrestrial Physics*, Vol. 44, 1982, pp. 461-469.

[22]Hung, R. J., Phan, T., and Smith, R. E., "Observation of Gravity Waves During the Extreme Tornado Outbreak of April 3, 1974," *Journal of Atmospheric and Terrestrial Physics*, Vol. 40, 1978, pp. 831-843.

[23]Hung, R. J., and Smith, R. E., "Ray Tracing of Gravity Waves as a Possible Warning System for Tornadic Storms and Hurricanes," *Journal of Applied Meteorology*, Vol. 17, 1978, pp. 3-11.

[24]Hung, R. J., and Kuo, J. P., "Ionospheric Observations of Gravity Waves Associated with Hurricane Eloise," *Journal of Geophysics*, Vol. 45, 1978, pp. 67-80.

[25]Hung, R. J., Tsao, Y. D., Johnson, D. L., Chen, A. J., Lin, C. H., Cheng, J. M., and You, C. M., "VHF Radar Remote Sensing of Atmospheric Parameters over Taiwan During the Time Period of Typhoon Wayne," *International Journal of Remote Sensing*, Vol. 9, 1988, pp. 477-493.

[26]Hung, R. J., Phan, T., and Smith, R. E., "Case Studies of Gravity Waves Associated with Isolated Tornadic Storms on January 13, 1976," *Journal of Applied Meteorology*, Vol. 18, 1979, pp. 460-466.

[27]Hung, R. J., Phan, R., and Smith, R. E., "Coupling of Ionosphere and Troposphere During the Occurrence of Isolated Tornadoes of November 20, 1973," *Journal of Geophysical Research*, Vol. 84, 1979, pp. 1261-1268.

[28]Hung, R. J., Phan, T., Lin, D. C., Smith, R. E., Jayroe, R. R., and West, G. S., "Gravity Waves and Goes IR Data Study of an

Isolated Tornadic Storm on 29 May 1977," *Monthly Weather Review*, Vol. 108, 1980, pp. 456-464.

[29]Hung, R. J., and Smith, R. E., "Ionospheric Remote Sensing of Medium-Scale Gravity Waves and Tornadic Storms, *Nuovo Cimento C*, Vol. 4, 1981, pp. 339-358.

[30]Hung, R. J., Phan, R., and Smith, R. E., "Ionosphere Doppler Sounder for Detection and Prediction of Severe Storms," *AIAA Journal*, Vol. 16, 1978, pp. 763-766.

[31]Dunkerton, T. J., "Stochastic Parameterization of Gravity-Wave Stresses," *Journal of Atmospheric Science*, Vol. 39, 1982, pp. 1711-1725.

[32]Schoeberl, M. R., Strobel, D. F., and Apruzese, J. P., "A Numerical Model of Gravity-Wave Breaking and Stress in the Mesosphere," *Journal of Geophysical Research*, Vol. 88, 1983, pp. 5249-5259.

[33]Baker, D. M., and Davies, K., "F2-Region Acoustic Waves from Severe Weather," *Journal of Atmospheric and Terrestrial Physics*, Vol. 31, 1969, pp. 1345-1352.

[34]Hung, R. J., and Smith, R. E., "Dynamics of Severe Storms Through the Study of Thermospheric-Tropospheric Coupling," *Journal of Geomagnetism and Geoelectricity*, Vol. 31, 1979, pp. 183-194.

[35]Gage, K. S., Carter, D. A., and Ecklund, W. L., "The Effect of Gravity Waves on Specular Echoes Observed by the Poker Flat MST Radar," *Geophysical Research Letters*, Vol. 8, 1981, pp. 599-602.

[36]Battan, L. J., *Radar Observations of the Atmosphere*, Univ. of Chicago Press, Chicago, IL, 1973.

[37]Hung, R. J., Dodge, J. C., and Smith, R. E., "The Life Cycle of a Tornadic Cloud as Seen from a Geosynchronous Satellite," *AIAA Journal*, Vol. 21, 1983, pp. 1217-1224.

[38]Crowley, G., Jones, T. B., Robinson, T. R., and Wade, N. M., "Determination of the Vertical Neutral Temperature and Wind Profiles Using EISCAT and HF Doppler Radar," *Journal of Atmospheric and Terrestrial Physics*, Vol. 46, 1984, pp. 501-507.

[39]Balsley, B. B., Ecklund, W. L., and Fritts, D. C., "VHF Echoes from the High Latitude Mesosphere and Lower Thermosphere: Observation and Interpretations," *Journal of Atmospheric Sciences*, Vol. 40, 1983, pp. 2452-2466.

[40]Fritts, D. C., and Rastogi, R. K., "Convective and Dynamical Instabilities Due to Gravity Wave Motions in the Lower and Middle Atmosphere: Theory and Observations," *Radio Science*, Vol. 20, 1985, pp. 1247-1278.

[41]Fritts, D. C., "Gravity Wave Saturation in the Middle Atmosphere: A Review of Theory and Observations," *Review of Geophysics and Space Physics*, Vol. 22, 1984, pp. 275-308.

Paul F. Mizera
Associate Editor